



OPEN ACCESS

EDITED BY

Giuseppe Failla,
Mediterranea University of Reggio
Calabria, Italy

REVIEWED BY

Zhengyong Song,
Xiamen University, China
Erkan Danaci,
TUBITAK National Metrology Institute
(NMI), Türkiye

*CORRESPONDENCE

Jaeyoung Choi,
✉ jychoi19@gachon.ac.kr
Dag Øivind Madsen,
✉ dag.oivind.madsen@usn.no

RECEIVED 02 October 2023

ACCEPTED 08 November 2023

PUBLISHED 21 November 2023

CITATION

Tiang JJ, Soliman NF, Khan I, Choi J,
Chung HC and Madsen DØ (2023),
Design and performance evaluation of a
novel broadband THz modulator based
on graphene metamaterial for
emerging applications.
Front. Mater. 10:1305793.
doi: 10.3389/fmats.2023.1305793

COPYRIGHT

© 2023 Tiang, Soliman, Khan, Choi,
Chung and Madsen. This is an open-
access article distributed under the terms
of the [Creative Commons Attribution
License \(CC BY\)](https://creativecommons.org/licenses/by/4.0/). The use, distribution or
reproduction in other forums is
permitted, provided the original author(s)
and the copyright owner(s) are credited
and that the original publication in this
journal is cited, in accordance with
accepted academic practice. No use,
distribution or reproduction is permitted
which does not comply with these terms.

Design and performance evaluation of a novel broadband THz modulator based on graphene metamaterial for emerging applications

Jun Jiat Tiang¹, Naglaa F. Soliman², Imran Khan^{3,4},
Jaeyoung Choi^{5*}, Hee Chan Chung⁵ and Dag Øivind Madsen^{6*}

¹Centre for Wireless Technology, Faculty of Engineering, Multimedia University, Cyberjaya, Malaysia, ²Department of Information Technology, College of Computer and Information Sciences, Princess Nourah bint Abdulrahman University, Riyadh, Saudi Arabia, ³Department of Electrical Engineering, University of Engineering and Technology, Peshawar, Pakistan, ⁴Islamic University Centre for Scientific Research, The Islamic University, Najaf, Iraq, ⁵School of Computing, Gachon University, Seongnam-si, Republic of Korea, ⁶University of South-Eastern Norway, Hønefoss, Norway

Introduction: Metamaterials consist of periodic arrangements of artificial subwavelength units that possess electromagnetic properties not present in natural media. It has attracted more interest due to its ability to alter electromagnetic radiation in a flexible manner, which has resulted in the development of multiple radio frequency devices based on metamaterials. Metamaterials with the required frequency band for electric or magnetic resonance can be made using unit cell structure. The incident electromagnetic wave will enter the metamaterials and be kept there in the absence of reflection.

Methods: This paper proposes a novel broadband THz absorber filter based on graphene for emerging applications. The proposed structure comprised of three parts. The top layer consists of graphene, the middle layer consists of dielectric and the bottom layer is made up of gold.

Results: The proposed structure is experimentally designed and validated using the COMSOL simulator.

Discussion: Simulation results show that the proposed absorber has better performance as compared with existing methods.

KEYWORDS

graphene, THz modulator, nanotechnology, computational optimization, absorber

1 Introduction

Terahertz absorbers have become a research hotspot in the field of terahertz and metamaterials due to their potential application value in detection, imaging and sensing. The huge application prospects of terahertz technology make it of great strategic significance in the future development of high-tech.

The terahertz band is located between visible light and infrared light, has rich spectrum resources, and has great strategic significance in fields such as communications (Olariu et al., 2023), biomedicine (Yin et al., 2022) and spectral detection (Liu et al., 2022). However, the lack of effective terahertz functional devices is one of the important factors limiting the development of

terahertz technology (Zhang et al., 2020; Chen et al., 2022a). Terahertz absorbers have received widespread attention in the fields of imaging (Sung et al., 2018), sensing (Wu et al., 2021) and stealth (Cheng et al., 2020). In practical applications, once a traditional terahertz absorber is manufactured, its structural size is fixed and it can only absorb terahertz waves of a specific frequency (Huang et al., 2021; Hossain et al., 2023). Therefore, it is particularly important to design a tunable high-performance terahertz absorber.

A brand-new class of electromagnetic materials created through artificial synthesis called metamaterials is made up of regular arrays of subwavelength unit structures. They typically consist of fundamental electric or magnetic resonance units and can cause electromagnetic waves to resonate in specific bands.

In order to adapt to more complex electromagnetic environments, many scholars have used temperature-sensitive, light-sensitive and magnetic-sensitive materials (Bing et al., 2019; Zheng et al., 2021; Ning et al., 2022). Among them, graphene, as a typical electrically tunable material, is composed of six carbon atoms in a hexagonal molecular structure (Nie et al., 2023). Graphene has unique high-mobility carriers, and the Fermi level can be precisely controlled by adding electrodes (Zhou and Song, 2022; Pan et al., 2023), and it has ultra-fast response from visible light to terahertz bands (Liu et al., 2021a). Due to its outstanding mechanical, optical, and electrical conductivity as well as its great carrier mobility, graphene has attracted a lot of attention. Therefore, the properties of graphene materials are very consistent with the requirements of tunable terahertz absorbers. Graphene and metamaterials are combined to design flexible tunable terahertz absorbers.

Different patterns of graphene excite plasmons at different resonant frequencies. There are two main design methods to achieve multi-peak or broadband absorption: The first is top-level plane design (Han and Chen, 2020; Zhang et al., 2021a), that is, designing structural units of different shapes and sizes on the top layer to generate resonance modes, and couple and superimpose each other to achieve broadband absorption. The second is vertical coupling design (Shen et al., 2020; Zhu et al., 2021), that is, hybridization and fusion between multi-layer structures to form multi-level resonance. The authors in (Fardoost et al., 2017) designed a 3-layer absorber with an annular porous graphene top layer. The simulation results showed that the absorption rate reached more than 90% in the range of 0.91–1.86 THz. In addition, by adding a layer of ring like porous graphene, the absorption bandwidth increases by 0.2 THz. Reference (Xie et al., 2021a) proposed an absorber composed of different geometric resonator structures. The absorber has a wide absorption bandwidth and achieves a broadband range of 1.26 THz (absorption > 80%). In the same year, a graphene layer absorber composed of a ring and a cross structure was proposed. There are fourth-order resonance and surface plasmon resonance in the 1.23 THz to 1.68 THz band, and its absorption rate reaches more than 99% (Feng et al., 2021). But so far, the absorption effect and width of graphene-based ultra-broadband perfect absorbers still need to be improved, and the device structure needs to be simplified.

This research work designed a graphene-based polarization-insensitive broadband THz absorber. The main contributions are as follows.

- The main structure from top to bottom is disk-shaped and L-shaped graphene, SiO₂ and metallic gold. By calculation through theoretical and simulation methods, it was found that

the absorption rate of the device exceeds 90% and reaches a spectrum width of 4.14 THz.

- The electromagnetic field distribution is used to specifically analyze the generation mechanism of broadband absorption, and the impact of changes in the geometric parameters of the device structure on the absorption performance is studied.
- The proposed design has great application potential, including smart switches, energy harvesting, modulators and filters.

The remaining of this paper is organized as follows. In Section 2, the proposed absorber model is described. Section 3 provides detailed simulation results evaluation while Section 4 gives the conclusion.

2 Model description

The proposed designed absorber is shown in Figure 1A. Among them, the graphene pattern on the top layer is shown in Figure 1B, which is mainly composed of L-shaped and circular shapes. Its optimized structural parameters are $P = 4 \mu\text{m}$, $L = 1.9 \mu\text{m}$, $R = 1.35 \mu\text{m}$. The middle layer is made of SiO₂ material with dielectric constant $\epsilon_s = 3.8$ and thickness $d = 7.5 \mu\text{m}$. The lower layer is made of metallic gold, with thickness $t = 2 \mu\text{m}$ and conductivity $\sigma = 4.09 \times 10^7 \text{ S/m}$ (Lan et al., 2022).

The absorber is simulated and its structural parameters are optimized through COMSOL simulation software. The absorptivity of the device $A = 1 - R - T$ (Li et al., 2022a; Zheng et al., 2023), where R and T are the reflectivity and transmittance of the device. To achieve perfect absorption, R , T need to be minimized, and the designed metal layer can effectively prevent the transmission of THz waves. That is, when $T = 0$, a reasonable model structure is illuminated by external electromagnetic waves, electromagnetic resonance will occur, that is, $R = 0$, thereby achieving perfect absorption (Zheng et al., 2022a).

To clearly reveal the principle of terahertz absorbers, multiple reflection interference theory (MRIT) is used (Chen, 2012; Yang et al., 2020). Figure 1C shows the propagation path of THz waves in the absorber. The terahertz wave enters the absorber obliquely from the air. Part of it is reflected on the upper surface of the graphene layer with a reflection coefficient of R_{12} , and the other part is transmitted into the SiO₂ layer with a transmission coefficient of T_{12} . When the THz wave transmitted into the SiO₂ layer reaches the metal layer, a complex phase factor will be added. After total reflection, after passing through the SiO₂ layer again, part of it is transmitted into the air. The amplitude of the transmitted terahertz wave at this time is $T_{12}T_{21}R_{23}e^{(2i\beta)}$, R_{23} is the reflection coefficient of the metal plate, and T_{21} is the THz wave incident from SiO₂ Transmission coefficient to air. Another part will undergo multiple reflections, and this superimposed multiple reflections can offset the direct reflections from the air and the graphene surface, thereby a high level of absorption is achieved. The total reflection coefficient of the device (Zhuo et al., 2022) can be expressed as:

$$R = R_{12} + T_{12}T_{21}R_{23}e^{(2i\beta)} + T_{12}T_{21}R_{21}R_{23}e^{(4i\beta)} + \dots \quad (1)$$

In the formula: $R_{23} = -1$; $\beta = \sqrt{\epsilon_s}k_0d$ is the propagation phase of the SiO₂ layer; k_0 is the size of the wave vector in free space. Simplifying Eq. 1 we get:

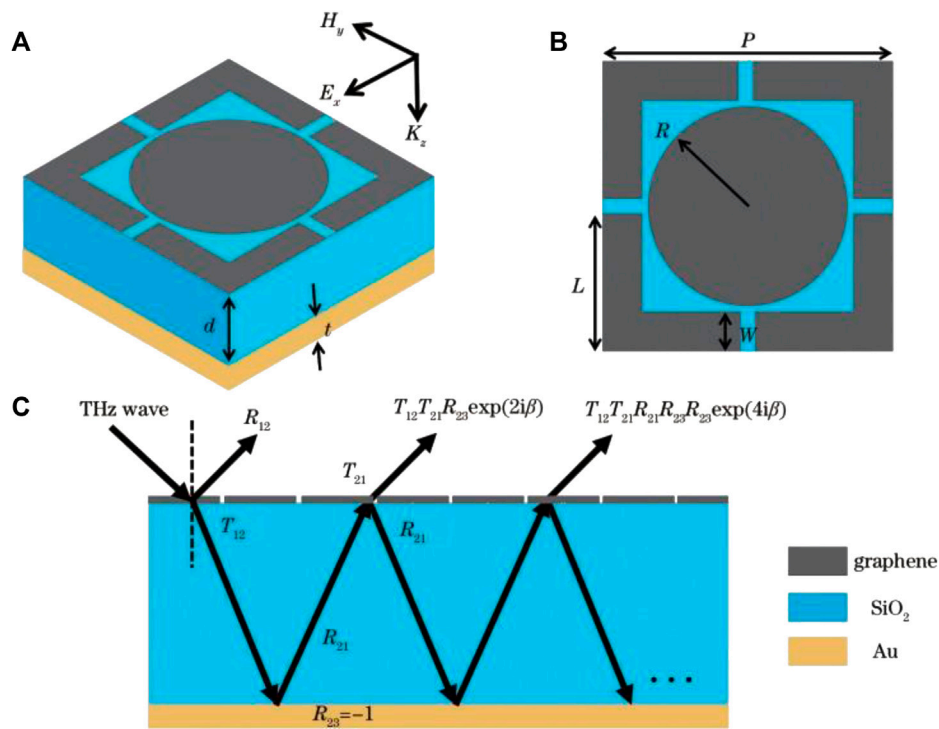


FIGURE 1
Proposed THz absorber design. (A) 3D-view; (B) top view; (C) wave propagation.

$$R \approx R_{12} - \frac{T_{12}T_{21}e^{(2i\beta)}}{1 + R_{21}e^{(2i\beta)}} \quad (2)$$

The total electrical conductivity σ of graphene is mainly composed of two parts: the intra-band electrical conductivity σ_{intra} and the inter-band electrical conductivity σ_{inter} (Xu et al., 2013; Pan et al., 2023). For the THz band at room temperature, according to the Pauli repulsion principle, σ_{intra} is negligible relative to σ_{inter} , so it is only necessary to mathematically solve σ_{inter} and convert it into Drude conductivity form. Therefore, σ (Andryieuski and Lavrinenko, 2013; Xu et al., 2013; Chen et al., 2021a) can be expressed as:

$$\sigma \approx \sigma_{\text{inter}} \approx \frac{ie^2|E_f|}{\pi h^2(\omega + \frac{i}{\tau})} \quad (3)$$

In the formula: τ is the relaxation time of graphene; E_f is the Fermi level of graphene; ω is the angular frequency of the incident THz wave; h is Planck's constant (1.05×10^{-34} J s); e is the electron charge (1.6×10^{-19} C). The relationship between the dielectric constant ϵ and conductivity σ of graphene (Chen et al., 2021a; Xie et al., 2021b) can be expressed as:

$$\epsilon = 1 + \frac{i\sigma}{\omega\epsilon_0 t_g} \quad (4)$$

In the formula: ϵ_0 is the dielectric constant in vacuum; t_g is the thickness of graphene. Graphene is a typical two-dimensional material, so the thickness of a single layer of graphene is set to 1 nm (Deng et al., 2016; Liu et al., 2021b; Qian et al., 2021; Lu et al.,

2022). In addition, the results of relevant research papers (Han and Chen, 2020; Li et al., 2021a; Liu et al., 2021c; Zheng et al., 2021) are reproduced to ensure the accuracy of the overall design method.

3 Results and discussion

Set graphene's $\tau = 0.1$ ps and $E_f = 0.95$ eV in the COMSOL simulator. When the incident electromagnetic wave is irradiated perpendicularly to the device, the absorption and reflection curve of the absorber at 2–8 THz is shown in Figure 2A. It can be seen from the dotted line in Figure 2A that the absorber has three peaks, and the absorption rate in the range of 3.02–7.16 THz exceeds 90%. The bandwidth of the absorber reaches 4.14 THz, and the relative bandwidth reaches 80%. The above greatly improves the performance of graphene-based tunable terahertz absorbers. It can be clearly seen that the simulated absorption spectrum has a very small deviation from the MRIT theoretical absorption spectrum. The main reason for the deviation is that the absorber is theoretically considered to have no loss. In addition, as shown in Figure 2B, the absorption effects on the transverse electric (TE) (the electric field of the external electromagnetic wave only exists in the y direction) and the transverse magnetic (TM) (the magnetic field only exists in the x direction) modes completely overlap, so the design structure is highly symmetrical on both the X-axis and Y-axis, and subsequent discussions will be conducted in TE mode.

To explore the intrinsic procedure, the absorption spectra of graphene layers with different patterns were drawn, as shown in Figure 3A.

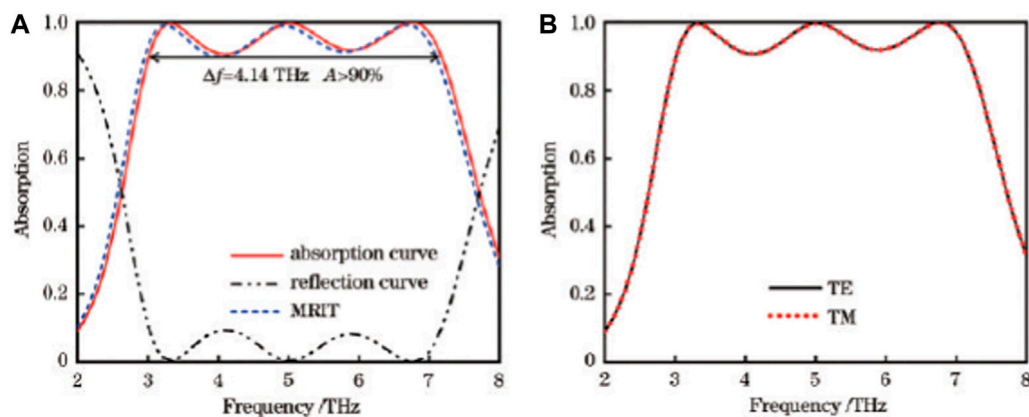


FIGURE 2

Results comparison of the proposed absorber. (A) Absorption, reflection and MRIT simulation; (B) TE and TM modes evaluation.

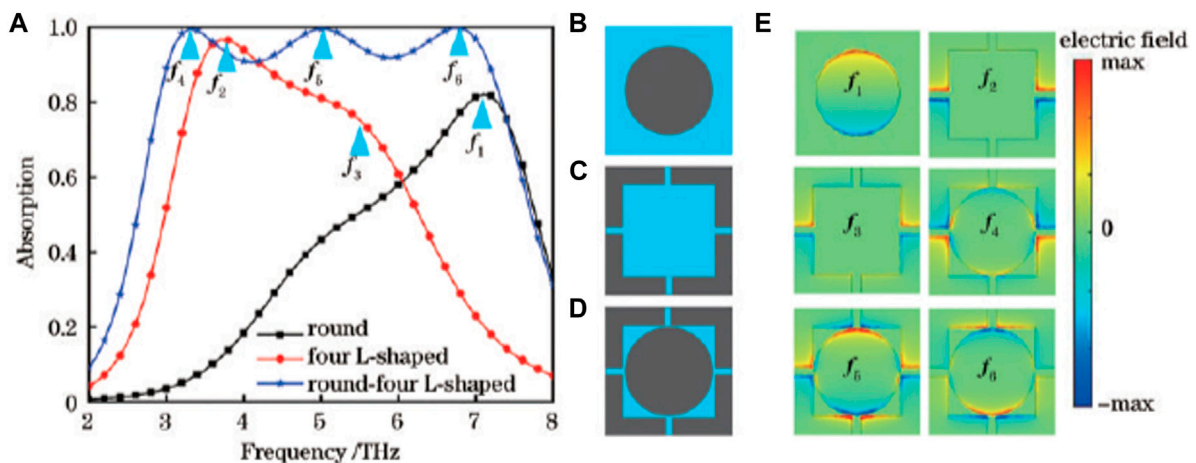


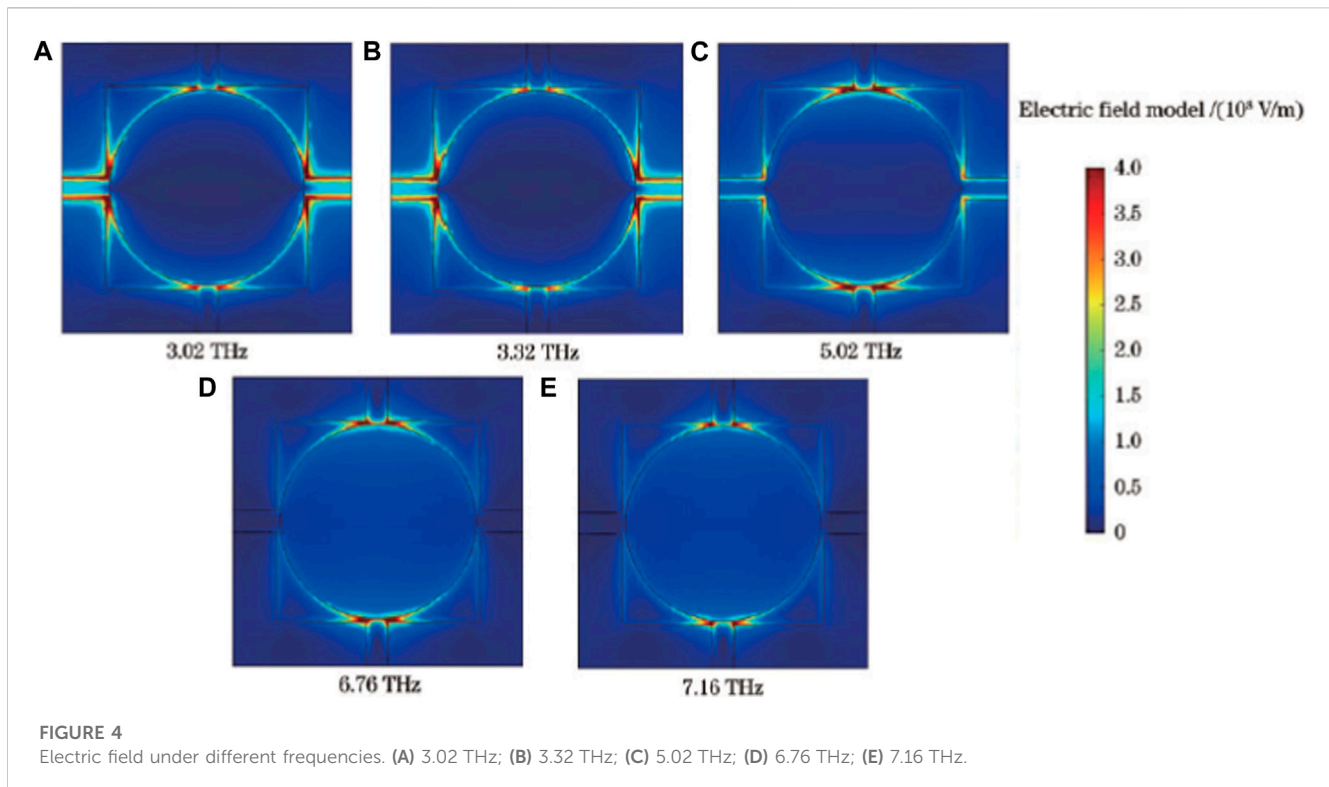
FIGURE 3

Absorption evaluation under different frequencies. (A) Absorption results of different shapes; (B) top view of circular design; (C) top view of four L-shaped design; (D) top view of circular and L-shaped design; (E) corresponding E-field in z direction.

The electric field distribution diagram (E_z) in the z direction at the marked frequency position in Figure 3A is shown in Figure 3E. Figures 3B–D are separate circles, four top views of two L-shaped and circular + L-shaped graphene absorbers. First, for the two separate arrays, the disk structure has a peak at the high-frequency position f_1 , and the absorption rate reaches 80%, while the overall L-shaped structure absorption is good, and there are two bumps at the low and mid-frequency positions (f_1 and f_3). The absorption produced by the two separate arrays is due to the weak surface plasmon excitation at the edge position of the graphene, forming a small number of dipole distributions along the direction of the incident electric field. For the combined structure, there are also three peaks, which may be caused by coupling between separate arrays. Combined with the electric field distribution diagram at each frequency in Figure 3E, the electric fields at f_1 and f_6 are distributed in the vertical direction, the electric fields at f_2 and f_4 are distributed in the horizontal direction, and the electric fields at f_3 and f_5 are distributed in the horizontal and vertical

directions. There is a partial electric field distribution. The L-shaped graphene layer is responsible for the absorption of the middle and low frequency bands, and the disk shape dominates the absorption of the middle and high frequency parts. There is a dipole distribution in the electric field at each frequency. This distribution causes a strong dipole resonance, which is related to the incident Electromagnetic waves act and lead to high absorption (Bordbar et al., 2020; Amin et al., 2021; Zhang and Song, 2021; Li et al., 2022b).

In addition, analyzing the electric field mode distribution $|E|$ of the absorber is also an important step in explaining the broadband absorber (Zhang et al., 2021b; Xu et al., 2021). Further, draw $|E|$ diagrams of the limit frequency (3.02, 7.16 THz) and 3 peak frequencies where the absorption rate is greater than 90%, as shown in Figure 4. At low frequencies (2.9, 3.32 THz), the electric field is mainly localized to the intersection of the horizontal slit of the cross structure and the disk shape (Cai et al., 2021; Miaofen et al., 2023). The graphene layer couples with the THz wave incident from the outside and it causes the



electric dipole resonance, so that the energy of the incident light is consumed in the SiO₂ layer, thereby achieving perfect absorption of the absorber (Bordbar et al., 2020; Zhang and Song, 2021). As the frequency increases, the local electric field gradually moves from the edge to the middle position (Yao et al., 2023). The electric field at the middle frequency position (5.02 THz) has been mostly localized to the slit of the disk and L-shaped combined structure along the direction of the electric field, and the electric field at the high frequency position (6.76, 7.16 THz) has been completely localized here. From the outside to the inside, the coupling between the electric dipole resonances at different positions is also an important reason for the generation of broadband absorption (Lu et al., 2017; Ding et al., 2023). This view can also be reflected from the absorption curve. To sum up, the ultra-broadband absorption produced by the device is caused by the mutual coupling between the dipoles generated by the two shapes of graphene and the dipole distribution generated at the main concentrated slits and their electric dipole resonance, namely, hybridization and coupling effects between combined structures (Wang et al., 2023; Zhao et al., 2023).

The designed absorber characteristics are further characterized by changing the shape of the internal graphene. As can be seen from Figure 5A, the internal absorption of circular, regular rhombus and octagonal graphene absorbers are shown in Figures 5B–D. The circular graphene changes into regular quadrilateral and regular octagonal graphene, and it can be found that the absorption rate of the absorber does not change much (An et al., 2023; Zhang et al., 2023). The slits generated by the coupling of L-shaped and other intermediate graphene shapes always exist, and most of the electromagnetic field should be strongly localized at the slits.

Therefore, a very efficient way to design ultra-broadband absorbers is to design different shapes of patterns on the top plane to construct air slits to form couplings, thereby increasing the FB and enhancing the absorption rate.

By changing the parameters of the absorber structure, the magnetic permeability and dielectric constant of graphene can be adjusted (Shi et al., 2023). In order for the absorber to maintain perfect absorption, its structural parameters need to be optimized. In addition, in the actual manufacturing process, it is difficult to accurately control the geometric parameters of the device, so the impact of geometric errors on device performance will be discussed later.

As shown in Figure 6A, as the thickness of the SiO₂ layer increases, the absorption curve gradually shifts to red. The absorption rate in the low-frequency part has always maintained an increasing trend. The peak at the intermediate frequency continues to maintain an absorption of more than 99%, while the high-frequency absorption peak first increases and then decreases. This is a change in SiO₂ thickness that causes the absorber's effective impedance and free space impedance to match each other at low and mid-range frequencies (Zhao et al., 2022), while matching and then breaking down at high frequencies. In Figures 6B–D, the effects of the radius *R* of the disk and the length *L* and width *W* of the L-shaped graphene on absorption are discussed respectively. As *R* increases, the absorption rate of the high-frequency part changes significantly, while the absorption effect of the mid- and low-frequency parts remains almost unchanged (Li et al., 2021b). As *L* becomes longer, the change in absorption rate is exactly the opposite, which also proves that the previously mentioned *L*

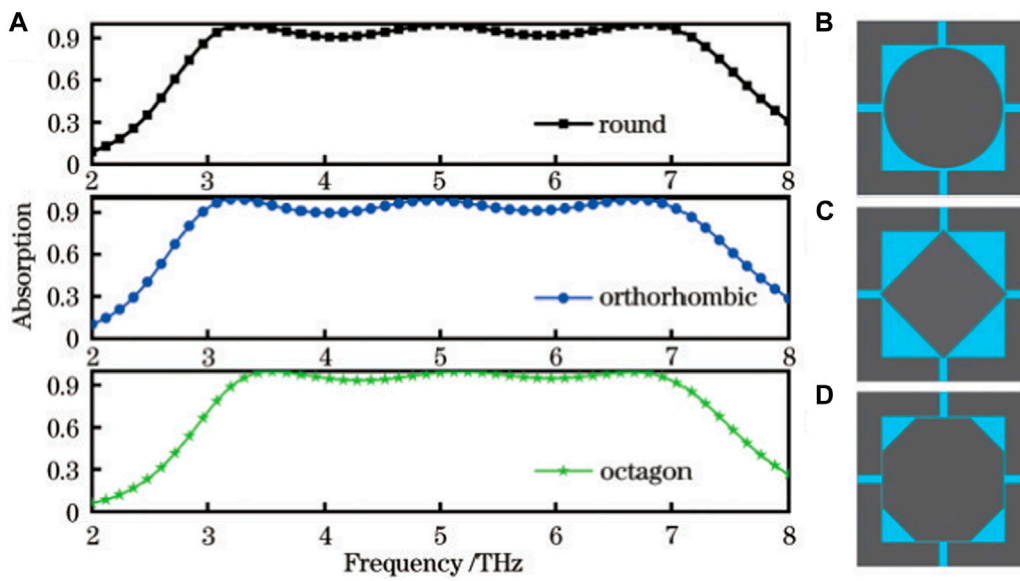


FIGURE 5 Comparison of absorption under different shapes. (A) Absorption evaluation; (B) circular; (C) quadrilateral; (D) octagonal.

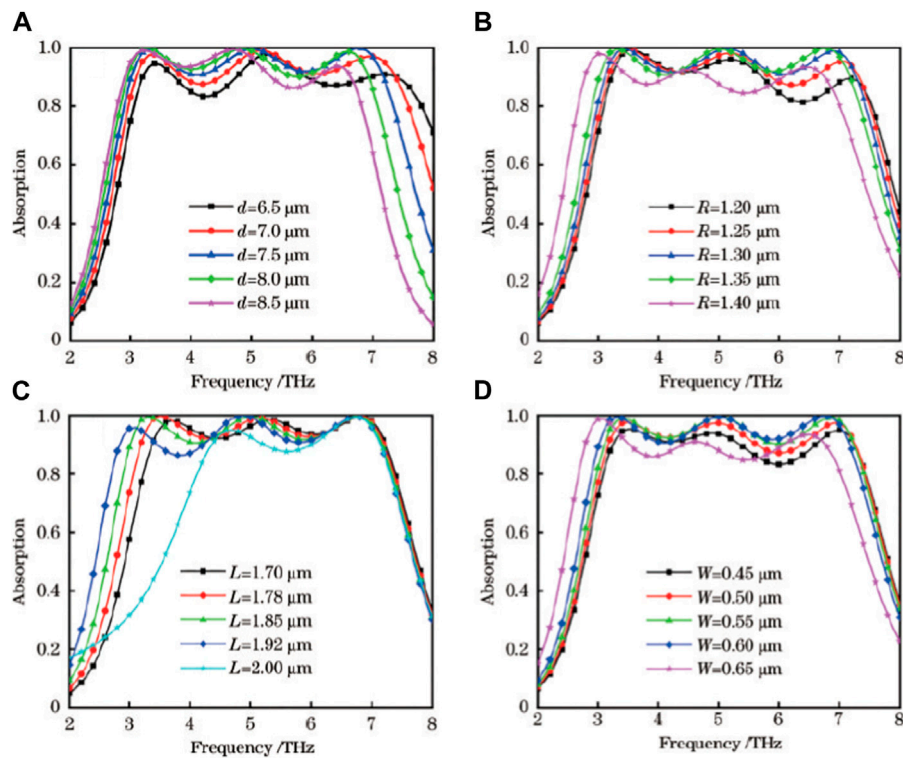


FIGURE 6 Impact of different geometrical parameters on absorption. (A) Variation with d ; (B) variation with R ; (C) variation with L ; (D) variation with W .

structure dominates the absorption of mid- to low-frequency parts, and the disk structure is responsible for the absorption of mid- and high-frequency parts. It can be seen from Figure 6D that when W changes from 0.45 to 0.60 μm , the absorption rate in

the entire frequency band continues to increase (Li et al., 2021c). Because the width of the L-shaped structure can also be defined as the distance between the L-shaped structure and the disk, as the distance decreases, the resonant coupling between the disk and

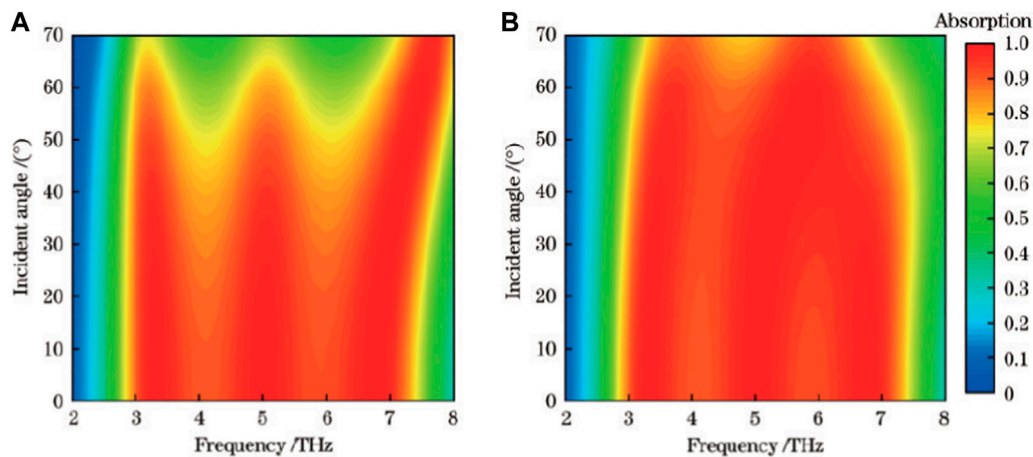


FIGURE 7 Impact of incident angle on absorption. (A) TE mode; (B) TM.

the L-shaped graphene increases, resulting in continued enhancement of the device's absorption rate. However, if the distance between the two is too small, the slit will become smaller, thereby reducing the local electric field and reducing the absorption rate. In summary, the structural parameters of the device can be changed within a certain range while maintaining high absorption, which will reduce the cost and difficulty in the actual manufacturing process.

During the actual use of the device, the THz wave incident from the outside is not necessarily perpendicular to the surface of the device, so it is very necessary to study the sensitivity of the polarization angle of the device. Figures 7A, B shows the absorption spectra of the device as the incident angle changes in TE and TM modes. In TE mode (Huang et al., 2023), when the incident angle changes from 0° to 70° and when it is 30°, the absorption intensity and spectrum width do not change much. As the incident angle continues to increase, the spectrum width and absorption rate slowly decrease until the incident angle is 50°, and the spectrum width with an absorption rate greater than 80% exceeds 4 THz (Lan et al., 2023). When the incident angle is greater than 50°, the absorption effect is significantly reduced, and the energy of the THz wave acting on the absorber surface is greatly reduced, so the absorption rate will decrease rapidly (Feng et al., 2021). In TM mode, when the incident angle is in the range of 0°–60°, the absorption effect and spectrum width are both very good, and when the electromagnetic wave is incident at an angle of 40°, its absorption effect is better than when it is vertically incident (Yang et al., 2023). This angle increases in TM mode, the dipoles on the surface of the absorber are effectively excited, which ultimately enhances the absorption effect. In summary, although the performance of the designed metamaterial will decrease as the incident angle increases, the designed absorber can still achieve very good absorption effects under wide-angle incidence in both polarization states.

The active tunable nature of the device will have more application space in practice. Figure 8 compared the impact of different E_f on the absorption. The Fermi level of graphene can be adjusted by applying an external DC bias voltage V_g using an ion gel

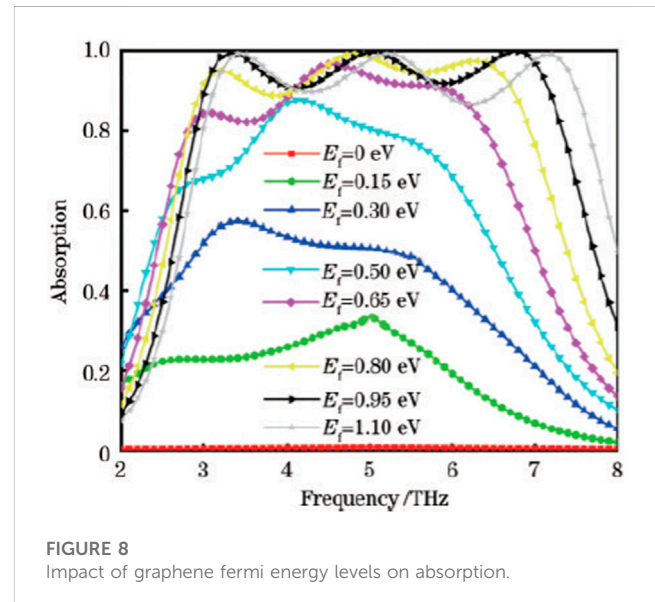


FIGURE 8 Impact of graphene fermi energy levels on absorption.

on the graphene layer, and the relationship (Amin et al., 2021; Pan et al., 2023) can be described as:

$$E_f = V_f \sqrt{\frac{\pi \epsilon_0 \epsilon_s V_g}{ed}} \quad (5)$$

In the formula: Fermi speed $V_f = c/300$. First, when $E_f = 0$ eV, the absorption rate of the absorber only reaches 1%, almost no absorption occurs (Chen et al., 2021b), and total reflection occurs on the surface of the upper graphene layer. When $E_f = 0.95$ eV, the absorber achieves ultra-wideband perfect absorption, and the device can be precisely controlled to flexibly switch between a perfect absorber and a complete reflector by applying an external voltage, which will make the designed absorption modulators play an important role in fields such as optical switches and modulators. In addition, as E_f continues to increase from 0 eV to 1.1 eV, the absorption curve continues to blue shift, and the size and bandwidth of the absorption rate also continue to increase. When $E_f = 0.95$ eV, the comprehensive effect of the absorption rate is the best

TABLE 1 Comparison of proposed and existing THz modulators.

Ref	FB (THz)	Layers	Modulation bandwidth (%)
Han and Chen (2020)	2.17	3	16 ~ 99
Fardoost et al. (2017)	1.15	5	55 ~ 99
Zheng et al. (2022b)	2.15	3	5 ~ 99
Chen et al. (2022b)	2.00	3	75 ~ 99
Liu et al. (2021d)	3.40	3	18 ~ 99
Proposed	4.06	3	1 ~ 99

(Li et al., 2022c). As E_f increases, more carriers can excite plasmons. In general, the designed absorber has active tunable properties and can better meet the requirements of practical applications.

Table 1 compared the performance parameters of the proposed design with other similar absorbers. The proposed design has a simple structure and far exceeds other similar absorbers in terms of bandwidth >90% (FB) and relative bandwidth, which can be deployed in emerging applications such as energy conversion and electromagnetic shielding.

4 Conclusion

In this article, a polarization-insensitive, functionally tunable and highly sensitive ultra-broadband absorber is designed based on graphene metamaterial. The proposed absorber dynamically alternates between ultra-wideband perfect absorption and total reflection by adjusting the applied voltage to change the Fermi level of graphene. When the Fermi level of graphene is adjusted to 0.95 eV, the absorption rate of the device is higher than 90% in the range of 3.02 ~ 7.16 THz. Through the analysis of electromagnetic field distribution ($|E|$ and E_z) and changing the shape of internal graphene, it is found that the coupling between the localized plasmon resonance at the slit and the electric dipole resonance is the main reason for producing broadband perfect absorption. Therefore, this research has broad application prospects in the fields of THz sensors, filters, smart switches, and also provides specific ideas for the design of THz ultra-wideband absorbers. The proposed absorber can be implemented using phase change material vanadium dioxide (VO_2).

Data availability statement

The original contributions presented in the study are included in the article/Supplementary material, further inquiries can be directed to the corresponding authors.

References

Amin, M., Siddiqui, O., Abutarboush, H., Farhat, M., and Ramzan, R. (2021). A THz graphene metasurface for polarization selective virus sensing. *Carbon* 176 (3), 580–591. doi:10.1016/j.carbon.2021.02.051

Author contributions

JT: Conceptualization, Methodology, Resources, Writing–original draft. NS: Data curation, Software, Validation, Visualization, Writing–original draft. IK: Data curation, Formal Analysis, Investigation, Supervision, Writing–review and editing. JC: Formal Analysis, Funding acquisition, Investigation, Methodology, Visualization, Writing–review and editing. HCC: Methodology, Validation, Writing, review and editing. DM: Funding acquisition, Methodology, Project administration, Resources, Supervision, Writing–original draft.

Funding

The authors would like to acknowledge the Princess Nourah bint Abdulrahman University Researchers Supporting Project number (PNURSP2023R66), Princess Nourah bint Abdulrahman University, Riyadh, Saudi Arabia. This work was supported by the National Research Foundation of Korea (NRF) grant funded by the Korean government (MSIT) (No. 2022R1C1C1004590).

Conflict of interest

The authors declare that the research was conducted in the absence of any commercial or financial relationships that could be construed as a potential conflict of interest.

Publisher's note

All claims expressed in this article are solely those of the authors and do not necessarily represent those of their affiliated organizations, or those of the publisher, the editors and the reviewers. Any product that may be evaluated in this article, or claim that may be made by its manufacturer, is not guaranteed or endorsed by the publisher.

An, Z., Huang, Y., and Zhang, R. (2023). High-temperature multispectral stealth metastructure from the microwave-infrared compatible design. *Compos. Part B Eng.* 259, 110737. doi:10.1016/j.compositesb.2023.110737

- Andryeuskii, A., and Lavrinenko, A. (2013). Graphene metamaterials based tunable terahertz absorber: effective surface conductivity approach. *Opt. Express* 21 (7), 9144–9155. doi:10.1364/oe.21.009144
- Bing, P., Guo, X., Wang, H., Li, Z., and Yao, J. (2019). Characteristic analysis of a photoexcited tunable metamaterial absorber for terahertz waves. *J. Opt.* 48, 179–183. doi:10.1007/s12596-019-00533-1
- Bordbar, A., Basiry, R., and Yahaghi, A. (2020). Design and equivalent circuit model extraction of a broadband graphene metasurface absorber based on a hexagonal spider web structure in the terahertz band. *Appl. Opt.* 59 (7), 2165–2172. doi:10.1364/ao.385476
- Cai, X., Tang, R., Zhou, H., Li, Q., Ma, S., Wang, D., et al. (2021). Dynamically controlling terahertz wavefronts with cascaded metasurfaces. *Adv. Photonics* 3 (3), 036003. doi:10.1117/1.ap.3.3.036003
- Chen, H., Chen, Z., Yang, H., Wen, L., Yi, Z., Zhou, Z., et al. (2022b). Multi-mode surface plasmon resonance absorber based on dart-type single-layer graphene. *RSC Adv.* 12 (13), 7821–7829. doi:10.1039/d2ra00611a
- Chen, L., Zhao, Y., Li, M., Li, L., Hou, L., and Hou, H. (2021b). Reinforced AZ91D magnesium alloy with thixomolding process facilitated dispersion of graphene nanoplatelets and enhanced interfacial interactions. *Mater. Sci. Eng. A* 804, 140793. doi:10.1016/j.msea.2021.140793
- Chen, T. (2012). Interference theory of metamaterial perfect absorbers. *Opt. Express* 20 (7), 7165–7172. doi:10.1364/oe.20.007165
- Chen, X., Chai, Q., Jin, M., and He, T. (2022a). Terahertz metamaterial absorbers. *Adv. Mater. Technol.* 7 (5), 2022, 2101171. doi:10.1002/admt.202101171
- Chen, Z., Chen, H., Yin, J., Zhang, R., Jile, H., Xu, D., et al. (2021a). Multi-band, tunable, high figure of merit, high sensitivity single-layer patterned graphene: perfect absorber based on surface plasmon resonance. *Diam. Relat. Mater.* 116, 108393. doi:10.1016/j.diamond.2021.108393
- Cheng, Y., Wang, Y., Niu, Y., and Zhao, Z. (2020). Concealed object enhancement using multi-polarization information for passive millimeter and terahertz wave security screening. *Opt. Express* 28 (5), 6350–6366. doi:10.1364/oe.384029
- Deng, B., Guo, Q., Li, C., Wang, H., Ling, X., Farmer, D. B., et al. (2016). Coupling-Enhanced broadband mid-infrared light absorption in graphene plasmonic nanostructures. *ACS Nano* 10 (12), 11172–11178. doi:10.1021/acsnano.6b06203
- Ding, G., Anselmi, N., Xu, W., Li, P., and Rocca, P. (2023). Interval-bounded optimal power pattern synthesis of array antenna excitations robust to mutual coupling. *IEEE Antennas Wirel. Propag. Lett.* 22 (11), 2725–2729. doi:10.1109/lawp.2023.3291428
- Fardoost, A., Vanani, F., Amirhosseini, A., et al. (2017). Design of a multilayer graphene-based ultrawideband terahertz absorber. *IEEE Trans. Nanotechnol.* 16 (1), 68–74. doi:10.1109/TNANO.2016.2627939
- Feng, H., Xu, Z., Li, K., Wang, M., Xie, W., Luo, Q., et al. (2021). Tunable polarization independent and angle-insensitive broadband terahertz absorber with graphene metamaterials. *Opt. Express* 29 (5), 7158–7167. doi:10.1364/oe.418865
- Han, J., and Chen, R. (2020). Tunable broadband terahertz absorber based on a single-layer graphene metasurface. *Opt. Express* 28 (20), 30289–30298. doi:10.1364/oe.403631
- Hossain, M., Rahman, M., and Faruque, M. (2023). An innovative polarisation-insensitive perfect metamaterial absorber with an octagonal-shaped resonator for energy harvesting at visible spectra. *Nanomaterials* 13 (12), 1882–1916. doi:10.3390/nano13121882
- Huang, M., Wei, K., Wu, P., Xu, D., and Xu, Y. (2021). Terahertz broadband absorber based on a combined circular disc structure. *Micromachines* 12 (11), 1290–1310. doi:10.3390/mi12111290
- Huang, X., Zhang, X., Zhou, L., Xu, J., and Mao, J. (2023). Low-loss self-packaged ka-band LTCC filter using artificial multimode SIW resonator. *IEEE Trans. Circuits Syst. II Express Briefs* 70 (2), 451–455. doi:10.1109/tcsii.2022.3173712
- Lan, G., Tang, L., Dong, J., Nong, J., Luo, P., Li, X., et al. (2023). Enhanced asymmetric light-plasmon coupling in graphene nanoribbons for high-efficiency transmissive infrared modulation. *China, Laser & Photonics Reviews*.
- Lan, J., Zhang, R., Bai, H., Zhang, C., Zhang, X., Hu, W., et al. (2022). Tunable broadband terahertz absorber based on laser-induced graphene. *Chin. Opt. Lett.* 20 (7), 073701. doi:10.3788/col202220.073701
- Li, A., Masouros, C., Swindlehurst, A. L., and Yu, W. (2021b). 1-Bit massive MIMO transmission: embracing interference with symbol-level precoding. *IEEE Commun. Mag.* 59 (5), 121–127. doi:10.1109/mcom.001.2000601
- Li, A., Masouros, C., Vucetic, B., Li, Y., and Swindlehurst, A. (2021c). Interference exploitation precoding for multi-level modulations: closed-form solutions. *IEEE Trans. Commun.* 69 (1), 291–308. doi:10.1109/tcomm.2020.3031616
- Li, M., Guo, Q., Chen, L., Li, L., Hou, H., and Zhao, Y. (2022c). Microstructure and properties of graphene nanoplatelets reinforced AZ91D matrix composites prepared by electromagnetic stirring casting. *J. Mater. Res. Technol.* 21, 4138–4150. doi:10.1016/j.jmrt.2022.11.033
- Li, T., Chen, H., Sun, A., Yang, X., Shangguan, Y., et al. (2022b). Microtopography-guided chessboard-like structure for a broadband terahertz absorber. *ACS Appl. Electron. Mater.* 4 (6), 2822–2830. doi:10.1021/acsaem.2c00325
- Li, Z., Xia, H., Zhao, Y., Lei, W., Zhao, C., and Xie, W., (2022a). Polarization-insensitive and absorption-tunable ultra-broadband terahertz metamaterial absorbers based on multiple resonant rings. *Results Phys.*, vol. 39, pp. 1–6. doi:10.1016/j.rinp.2022.105786
- Li, Z., Yi, Z., Liu, T., Liu, L., Chen, X., Zheng, F., et al. (2021a). Three-band perfect absorber with high refractive index sensing based on an active tunable Dirac semimetal. *Phys. Chem. Chem. Phys. PCCP* 23 (32), 17374–17381. doi:10.1039/d1cp01375k
- Liu, M., Guo, L., and Zhang, M. (2021d). Analytical method for designing tunable terahertz absorbers with the desired frequency and bandwidth. *Opt. Express* 29 (24), 39777–39787. doi:10.1364/oe.442425
- Liu, W., Lv, Y., Tian, J., and Yang, R. (2021c). A compact metamaterial broadband THz absorber consists of graphene crosses with different sizes. *Superlattices Microstruct.* 159, 107038. doi:10.1016/j.spmi.2021.107038
- Liu, W., Xu, J., and Song, Z. (2021a). Bifunctional terahertz modulator for beam steering and broadband absorption based on a hybrid structure of graphene and vanadium dioxide. *Opt. Express* 29 (15), 23331–23340. doi:10.1364/oe.433364
- Liu, W., Zhang, L., Su, Q., Xu, Q., Guo, L., Yu, Z., et al. (2022). Interdigitated photoconductive antenna-based two-color femtosecond laser filamentation THz time-domain spectral detection. *Opt. Express* 30 (11), 18562–18570. doi:10.1364/oe.456194
- Liu, Y., Huang, R., and Ouyang, Z. (2021b). Terahertz absorber with dynamically switchable dual-broadband based on a hybrid metamaterial with vanadium dioxide and graphene. *Opt. Express* 29 (13), 20839–20850. doi:10.1364/oe.428790
- Lu, Y., Liu, W., Tian, J., and Yang, R. (2022). Broadband terahertz metamaterial absorber and modulator based on hybrid graphene-gold pattern. *Phys. E Low-Dimensional Syst. Nanostructures* 140, 115142. doi:10.1016/j.physe.2022.115142
- Lu, Y., Stegmaier, M., Nukala, P., Giambra, M. A., Ferrari, S., Busacca, A., et al. (2017). Mixed-mode operation of hybrid phase-change nanophotonic circuits. *Nano Lett.* 17 (1), 150–155. doi:10.1021/acs.nanolett.6b03688
- Miaofen, L., Youmin, L., Tianyang, W., Fulei, C., and Zhike, P. (2023). Adaptive synchronous demodulation transform with application to analyzing multicomponent signals for machinery fault diagnostics. *Mech. Syst. Signal Process.* 191, 110208. doi:10.1016/j.ymssp.2023.110208
- Nie, R., He, C., Zhang, R., and Song, Z. (2023). Vanadium dioxide-based terahertz metasurfaces for manipulating wavefronts with switchable polarization. *Opt. Laser Technol.* 159, 109010. doi:10.1016/j.optlastec.2022.109010
- Ning, J., Chen, K., Zhao, W., Zhao, J., Jiang, T., and Feng, Y. (2022). An ultrathin tunable metamaterial absorber for lower microwave band based on magnetic nanomaterial. *Nanomaterials* 12 (13), 2135–2214. doi:10.3390/nano12132135
- Olariu, T., Beck, M., and Faist, J. (2023). Post-process frequency tuning of single-mode quantum cascade laser at 4.7 THz. *IEEE J. Quantum Electron.* 59 (5), 1–7. doi:10.1109/jqe.2023.3295402
- Pan, Z., Zhou, Z., and Song, Z. (2023). Terahertz generations of transmissive deflection, focusing, and orbital angular momentum with polarization conversion. *Opt. Laser Technol.* 159, 109036. doi:10.1016/j.optlastec.2022.109036
- Qian, J., Zhou, J., Zhu, Z., Ge, Z., Wu, S., Liu, X., et al. (2021). Polarization-insensitive broadband THz absorber based on circular graphene patches. *Nanomaterials* 11 (10), 2709–2713. doi:10.3390/nano11102709
- Shen, H., Liu, F., Liu, C., Zeng, D., Guo, B., Wei, Z., et al. (2020). A polarization-insensitive and wide-angle terahertz absorber with ring-porous patterned graphene metasurface. *Nanomaterials* 10 (7), 1410–1411. doi:10.3390/nano10071410
- Shi, J., Li, Z., Jia, J., Li, Z., Shen, C., Zhang, J., et al. (2023). Waveform-to-Waveform end-to-end learning framework in a seamless fiber-terahertz integrated communication system. *J. Light. Technol.* 41 (8), 2381–2392. doi:10.1109/jlt.2023.3236400
- Sung, S., Dabironezare, S., Llombart, N., Brown, E., Grundfest, W. S., Taylor, Z. D., et al. (2018). Optical system design for noncontact, normal incidence, THz imaging of *in vivo* human cornea. *IEEE Trans. Terahertz Sci. Technol.* 8 (1), 1–12. doi:10.1109/tthz.2017.2771754
- Wang, Q., Li, P., Rocca, P., Li, R., Tan, G., Hu, N., et al. (2023). Interval-based tolerance analysis method for petal reflector antenna with random surface and deployment errors. *IEEE Trans. Antennas Propag.* 71 (11), 8556–8569. doi:10.1109/tap.2023.3314097
- Wu, L., Zheng, Y., Luo, Y., Zhang, J., Yi, Z., Wu, X., et al. (2021). A four-band and polarization-independent BDS-based tunable absorber with high refractive index sensitivity. *Phys. Chem. Chem. Phys. PCCP* 23 (47), 26864–26873. doi:10.1039/d1cp04568g
- Xie, T., Chen, D., Yang, H., et al. (2021a). Tunable broadband terahertz waveband absorbers based on fractal technology. *Nanomaterials* 11 (2), 1–13.
- Xie, T., Chen, D., Yang, H., Xu, Y., Zhange, Z., and Yang, J. (2021b). Tunable broadband terahertz waveband absorbers based on fractal technology of graphene metamaterial. *Nanomaterials* 11 (2), 269–313. doi:10.3390/nano11020269
- Xu, B., Gu, Q., Li, Z., and Niu, Z. y. (2013). A novel structure for tunable terahertz absorber based on graphene. *Opt. Express* 21 (20), 23803–23811. doi:10.1364/oe.21.023803
- Xu, K., Guo, Y., Liu, Y., Deng, X., Chen, Q., and Ma, Z. (2021). 60-GHz compact dual-mode on-chip bandpass filter using GaAs technology. *IEEE Electron Device Lett.* 42 (8), 1120–1123. doi:10.1109/led.2021.3091277

- Yang, D., Zhang, C., Ju, X., Ji, Y., and Lan, C. (2020). Multi-resonance and ultra-wideband terahertz metasurface absorber based on micro-template-assisted self-assembly method. *Opt. Express* 28 (2), 2547–2556. doi:10.1364/oe.381927
- Yang, M., Cai, C., Wang, D., Wu, Q., Liu, Z., and Wang, Y. (2023). Symmetric differential demodulation-based heterodyne laser interferometry used for wide frequency-band vibration calibration. *IEEE Trans. Industrial Electron.*, 1–9. doi:10.1109/TIE.2023.3299015
- Yao, H., Sun, Z., Liang, L., Yan, X., Wang, Y., Yang, M., et al. (2023). Hybrid metasurface using graphene/graphitic carbon nitride heterojunctions for ultrasensitive terahertz biosensors with tunable energy band structure. *Photonic Res.* 11 (5), 858–868. doi:10.1364/prj.482256
- Yin, X., Wadji, A., and Zhang, Y. (2022). A biomedical perspective in terahertz nano-communications: a review. *IEEE Sensors J.* 22 (10), 9215–9227. doi:10.1109/jsen.2022.3161013
- Zhang, M., and Song, Z. (2021). Switchable terahertz metamaterial absorber with broadband absorption and multiband absorption. *Opt. Express* 29 (14), 21551–21561. doi:10.1364/oe.432967
- Zhang, Q., Xu, Q., Xia, L., Li, Y., Gu, J., Tian, Z., et al. (2020). Terahertz surface plasmonic waves: a review. *Adv. Photonics* 2 (1), 014001. doi:10.1117/1.ap.2.1.014001
- Zhang, R., Luo, Y., Xu, J., Wang, H., Han, H., Hu, D., et al. (2021a). Structured vanadium dioxide metamaterial for tunable broadband terahertz absorption. *Opt. Express* 29 (26), 42989–42998. doi:10.1364/oe.447949
- Zhang, Y., He, Y., Wang, H., Sun, L., and Su, Y. (2021b). Ultra-broadband mode size converter using on-chip metamaterial-based luneburg lens. *ACS Photonics* 8 (1), 202–208. doi:10.1021/acsp Photonics.0c01269
- Zhang, Y., Zhao, P., Lu, Q., Zhang, Y., Lei, H., Yu, C., et al. (2023). Functional additive manufacturing of large-size metastructure with efficient electromagnetic absorption and mechanical adaptation. *Compos. Part A Appl. Sci. Manuf.* 173, 107652. doi:10.1016/j.compositesa.2023.107652
- Zhao, J., Zhou, M., Chen, J., Wang, L., Zhang, Q., Zhong, S., et al. (2023). Two birds one stone: graphene assisted reaction kinetics and ionic conductivity in phthalocyanine-based covalent organic framework anodes for lithium-ion batteries. *Nano-Micro Small* 19 (44), 2303353. doi:10.1002/smll.202303353
- Zhao, Z., Xu, G., Zhang, N., and Zhang, Q. (2022). Performance analysis of the hybrid satellite-terrestrial relay network with opportunistic scheduling over generalized fading channels. *IEEE Trans. Veh. Technol.* 71 (3), 2914–2924. doi:10.1109/tvt.2021.3139885
- Zheng, L., Feng, R., Shi, H., and Li, X. (2023). Tunable broadband terahertz metamaterial absorber based on vanadium dioxide and graphene. *Micromachines* 14 (9), 1715–1812. doi:10.3390/mi14091715
- Zheng, P., Luo, Y., Yang, H., Yi, Z., Zhang, J., Song, Q., et al. (2022b). Thermal tuning of terahertz metamaterial absorber properties based on VO₂. *Phys. Chem. Chem. Phys.* PCCP 24 (15), 8846–8853. doi:10.1039/d2cp01070d
- Zheng, P., Zheng, Y., Luo, Y., Yi, Z., Zhang, J., Liu, L., et al. (2021). Terahertz perfect absorber based on flexible active switching of ultra-broadband and ultra-narrowband. *Opt. Express* 29 (26), 42787–42799. doi:10.1364/oe.445155
- Zheng, P., Zheng, Y., Luo, Y., Yi, Z., Zhang, J., Liu, Z., et al. (2022a). A switchable terahertz device combining ultra-wideband absorption and ultra-wideband complete reflection. *Phys. Chem. Chem. Phys.* PCCP 24 (4), 2527–2533. doi:10.1039/d1cp04974g
- Zhou, Z., and Song, Z. (2022). Terahertz mode switching of spin reflection and vortex beams based on graphene metasurfaces. *Opt. Laser Technol.* 153, 2022, 108278. doi:10.1016/j.optlastec.2022.108278
- Zhu, J., Wu, C., and Ren, Y. (2021). Broadband terahertz metamaterial absorber based on graphene resonators with perfect absorption,” *Results Phys.*, vol. 26, pp. 1–7. doi:10.1016/j.rinp.2021.104466
- Zhuo, S., Zhou, F., Liu, Y., Liu, Z., Zhang, X., Luo, X., et al. (2022). Terahertz multimode modulator based on tunable triple-plasmon-induced transparency in monolayer graphene metamaterials. *J. Opt. Soc. Am. A* 39 (4), 594–599. doi:10.1364/josaa.452393